

Laboratory and numerical experiments on propagation of high-power femtosecond laser radiation through air and droplet media

S.N. Bagaev,² Yu.E. Geints,¹ A.A. Zemlyanov,^{1,4} A.M. Kabanov,¹
G.G. Matvienko,¹ E.V. Pestryakov,² A.N. Stepanov,³ and V.I. Trunov²

¹*Institute of Atmospheric Optics,
Siberian Branch of the Russian Academy of Sciences, Tomsk*

²*Institute of Laser Physics,*

Siberian Branch of the Russian Academy of Sciences, Novosibirsk

³*Institute of Applied Physics, Russian Academy of Sciences, Nizhni Novgorod*

⁴*Tomsk State University*

Received February 21, 2007

We present the results of experimental and numerical study of self-focusing and filamentation of high-power femtosecond laser radiation in pure air and droplet medium. Measured data are presented on energy transmission, pulse spectral content, and transverse profile of the laser beam energy density at different points of the optical path in the air. Discussion of the results is based on formalism of the laser beam effective (integral) parameters. It is found that the femtosecond radiation attenuation in water aerosol occurs as in the case under linear conditions. A similarity of evolution of the effective laser beam radius is established under conditions of single and multiple filamentation. The correlation between the path length of the light beam filamentation and effective width of its frequency spectrum is shown.

Introduction

Development of femtosecond laser systems during the past two decades yielded new research areas and technologies.^{1,2} The investigation of interaction between the femtosecond laser pulses of terawatt power^{2,3} and atmospheric components^{4,5} is of a special interest. Studying of high-power laser radiation propagation of femtosecond duration¹⁻³ in the atmosphere is important for a series of practical applications, such as formation of the extended ionized channel in the atmosphere,⁶ multicomponent detection of contaminants,⁷ luminous energy transmission,⁸ electromagnetic pulse generation in the terahertz range.⁹

It is known that the laser pulses of femtosecond duration propagating through the atmosphere with initial peak power exceeding a critical value, the beam filamentation takes place, which is connected with strong spatiotemporal self-modulation of light wave. The light filament is an optical waveguide. Its mean diameter in the atmospheric air for radiation with $\lambda_0 = 800$ nm is about 100 μm , and the peak intensity is of 10^{14} W/cm². The mean filament length on a horizontal atmospheric path is, as a rule, tens of meters.¹⁰ The femtosecond beam filamentation is accompanied by generation of supercontinuum radiation (SC). It is experimentally found that the SC spectrum covers the UV- and near-IR spectral region.¹¹

The physical pattern of the high-power ultrashort laser pulse filamentation in the atmosphere and formation of SC radiation has been presented in

numerous experimental and theoretical studies.^{3,12} A wide set of optical radiation parameters, which are characterized by the broad variation range depending on the path length and propagation conditions, is measured, as a rule, in field and laboratory experiments. Therefore, the problem is in optimal set of parameters, which characterize the process and that would make it possible to construct versatile relations for the case of unsteady self-action conditions. In other words, it is necessary to find the similarity parameters of the problem.

One can solve this problem under controlled laboratory conditions in combination with the corresponding similarity theory. An appropriate self-action theory is based on studying the evolution of effective (integral) characteristics of laser beams. The global light beam transformations in the medium are described. The spatiotemporal radiation structure affects the behavior of its integral parameters that allows obtaining the similarity relations for various unsteady self-action conditions.

In this study we present data of laboratory experimental research into the propagation of high-power femtosecond focused pulses of a Ti:Sa laser in air and droplet media. Pulse energy varied so that a laser beam could be subjected to either single or multiple filamentation. The measurements of energy transmission, pulse spectral content, cross profile of laser beam energy density were carried out at different points along the optical path. To analyze the experimental data, the formalism of radiation integral parameters was used, which allowed determining the

typical scales of complex multimode distributions of measured laser radiation characteristics. The dependences of the effective laser radiation parameters obtained in the experiment were compared with the numerical modeling results on the femtosecond pulse filamentation in air.

Experimental complex

Two experimental set-ups with the femtosecond laser system designed at the Institute of Applied Physics (IAP RAS) and Institute of Laser Physics (ILP SB RAS) were used in the experiment.

The basic arrangement that is being employed nowadays to obtain terawatt power in laser systems uses amplification of the preliminary time-extended frequency-modulated laser pulses from a master oscillator with their subsequent compression, the so-called scheme of *chirped pulse amplification* (CPA).

The master oscillator³ designed at IAP RAS, is a sapphire crystal laser, doped with titanium (Ti:Sa), with passive mode synchronization due to the Kerr mechanism, whose basic scheme can be found in numerous publications on femtosecond lasers. The spatial single mode radiation of the second harmonics of the continuous-wave solid-state laser is used as a femtosecond laser pumping ("Spectra Physics" Company, "Millenia" model). The mean power of output radiation was about 600–700 mW at pulse repetition frequency equal to ~ 80 MHz and pulse duration ~ 50 fs. After the master oscillator, the femtosecond laser pulses were extended in the stretcher, made from two spherical mirrors and diffraction grating according to the Offner scheme. Amplification of the time-extended laser pulses occurs sequentially in regenerative and four-pass amplifiers (second harmonics radiation of the "Quanta Ray" laser by the "Spectra Physics" company was used as pumping with pulse energy $E_0 \leq 200$ mJ). After the compressor constructed using single-grating scheme, the pulses with $t_p \approx 80$ fs and $E_0 \leq 20$ mJ were obtained at the laser system output. The laser system operates in a frequency mode with pulse repetition frequency of 10 Hz and in a single pulse mode. The radiation spectrum width Δ_λ for nano- and femtosecond pulses at the half-maximum makes 15–20 nm that allows comparing the qualitative and quantitative differences at interaction between nano- and femtosecond pulses and the propagation medium. The intensity distribution across the beam is close to that of Gaussian width at the level of 0.135 of the peak value makes about 8 mm.

The terawatt femtosecond laser system designed at ILP SB RAS [Ref. 2] operates in the region of 800 nm and delivers pulses with $E_0 = 60$ mJ and $t_p = 50$ fs at the pulse repetition frequency of 10 Hz. The system includes a master oscillator and two amplifiers based on regenerative and multipass amplifiers. A "Mira" Ti:Sa laser pumped by the "Verdi" laser (Coherent, USA) is used as a master oscillator. The femtosecond laser pulses are extended in the stretcher and amplified in the regenerative amplifier

"Legend" (Coherent, USA) based on the $\text{Al}_2\text{O}_3:\text{Ti}^{3+}$ crystal pumped by the second harmonics radiation of the Nd:YLF laser (Evolution-30) up to the energy of 1–2 mJ. Radiation of the amplified chirped pulses with a pulse repetition frequency of 1 kHz after the telescope reducing the beam diameter to 4 mm, passes through the electrooptical modulator, which separates each 100th pulse. Further, these pulses are amplified in a four-pass amplifier pumped from both sides by the second harmonics pulses of the Nd:YAG laser LQ-929 (Solar, Byelorussia) with duration of 15–20 ns and energy up to 800 mJ, and then are applied to the compressor. The compressor is constructed using two-grating scheme (two holographic gratings with 1400 grooves/mm. Parameters of the amplified and compressed pulses are controlled by the single pulse autocorrelator ASF-20T with the front tilt measurement and the phase characteristics meter of the femtosecond pulses SPIDER SP-120 (Avesta, Russia).

Effective parameters of a laser pulse

The effective parameters of a light beam are determined by its local characteristics and introduced by the following expressions.^{8,13,14}

Energy transmission coefficient:

$$T_e(z) = E(z)/E_0.$$

The root-mean-square half-width of the radiation frequency spectrum Δ_λ :

$$\Delta_\lambda(z) = \left[\frac{1}{E(z)} \int_{\Lambda} F(\lambda, z) (\lambda - \lambda_{\text{gr}})^2 d\lambda \right]^{1/2}.$$

Effective (energy) beam radius R_e :

$$R_e(z) = \left[\frac{1}{E(z)} \iint_{\mathbf{R}_\perp} d^2\mathbf{r}_\perp W(\mathbf{r}_\perp, z) |\mathbf{r}_\perp - \mathbf{r}_{\text{gr}}|^2 \right]^{1/2}, \quad (1)$$

where F is the energy per unit spectral interval, J/m; W is the density of radiation energy within the beam cross section, J/m²;

$$E = \iint_{\mathbf{R}_\perp} d^2\mathbf{r}_\perp W(\mathbf{r}_\perp, z) = \int_{\Lambda} F(\lambda, L) d\lambda$$

is the total pulse energy; Λ , \mathbf{R}_\perp are the spectral interval and spatial domain, where the measurements of quantities were carried out; L is the path length;

$$\lambda_{\text{gr}}(z) = \frac{1}{E(z)} \int_{\Lambda} F(\lambda, z) \lambda d\lambda$$

is the gravity center of the radiation spectrum;

$$\mathbf{r}_{\text{gr}} = \frac{1}{E(z)} \iint_{\mathbf{R}_\perp} W(\mathbf{r}_\perp, z) \mathbf{r}_\perp d^2\mathbf{r}_\perp$$

is the radius-vector of the gravity center of cross profile of the beam energy density; λ is the wavelength; \mathbf{r}_\perp , z are the transverse and longitudinal coordinates.

Energy attenuation of the femtosecond laser pulse in water aerosol

The source of laser pulses is a laser complex (IAP RAS). Transmission T_e of the model aerosol layer (length along the laser radiation propagation is 1.2 cm), made of monodisperse water drops of 2.5 μm radius, was measured at two wavelengths: acting high-power laser pulse with $\lambda_0 = 800$ nm and sounding low-power continuous radiation of a He-Ne laser at $\lambda_0 = 630$ nm. The co-axial introduction of sounding radiation with known attenuation coefficient in water aerosol was required for control of concentration N of the particles in aerosol medium for each pulse of the Ti:Sa laser. The energy variation control of the femtosecond pulse E_0 was conducted by the reference signal and measurements of an auxiliary photodiode, whose response was calibrated against the pulse energy measurements for each measurement series.

Relation of the Ti:Sa laser signal, passed through the aerosol layer, to the reference signal (without aerosol), showing transparency of the medium for the given wavelength, was adjusted by the relation of reference signals for each shot by the corresponding coefficient. Figure 1 presents the measured results of aerosol transmission depending on concentration of particles.

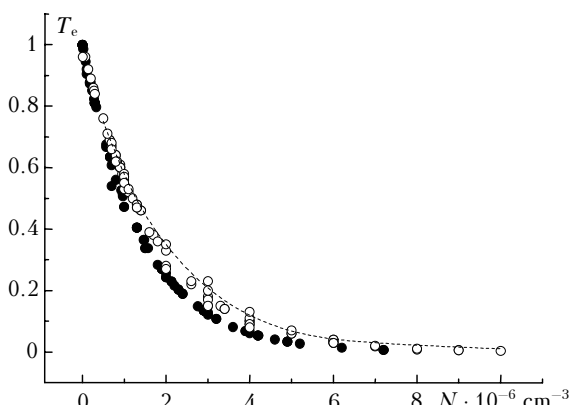


Fig. 1. Dependence of optical transmission of aerosol layer T_e on concentration of water particles N : ● is the transmission for continuous radiation ($\lambda_0 = 630$ nm); ○ is for the femtosecond pulse ($E_0 = 9$ mJ). Dot line denotes calculation by the Bouguer formula for $\lambda_0 = 800$ nm.

It turned out that in spite of the fixed optical breakdown inside the aerosol particles, and the essential increase in the acoustic signal amplitude from aerosol at laser pulse propagation of femtosecond duration, the nonlinear interaction with atmospheric aerosol does not affect significantly the energy characteristics of femtosecond radiation passed through the aerosol region.⁵

The transmission coefficient of aerosol layer shows the exponential decay with growth of aerosol optical density that is typical for the situation of linear radiation attenuation in a disperse medium, described by the Bouguer's law.

Spectral characteristics of femtosecond pulse in the air

The processing of experimental data on the spectral contours of SC, and the cross profile of the femtosecond beam energy density was conducted in the following way. At the first stage, the background and noise signal components were subtracted out of the raw experimental data by means of the digital spectral filtration. Then, the filtered data were analyzed in a computer using specialized software package computing the peak and averaged characteristics of the measured profiles. The spectral measurements at laser pulse filamentation of a femtosecond duration were conducted over the range of pulse energies from 0.1 to 18 mJ with an S-150 spectrometer (Fig. 2a) and with the use of the integrating sphere of an S-2000 spectrometer at radiation focusing by lenses with a focal length of 390 and 60 mm (Fig. 2b).

Radiation spectral contour expands at the initial beam filamentation both to the blue and red regions relative to the central wavelength. Hence, not only the spectral distribution half-width changes, but also its shape, which acquires the more expressed blue wing. This fact specifies gas ionization and plasma emergence in the laser beam channel. Owing to this fact, the gravity center of the radiation spectral contour λ_{gr} is shifted to the short-wave region.

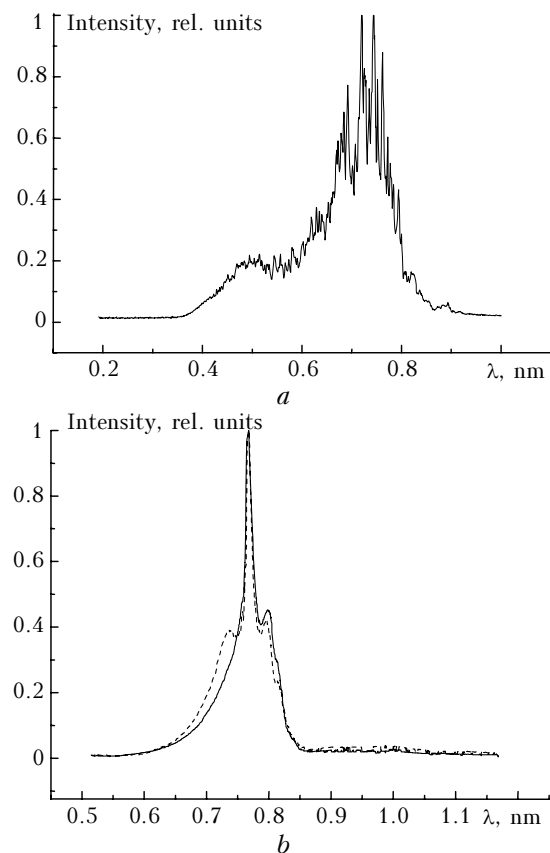


Fig. 2. The shape of SC spectra of the filamented laser beam: $t_p = 80$ fs, $E_0 = 15$ mJ, $F = 860$ mm, S-150 spectrometer (a); $t_p = 50$ fs, $E_0 = 18$ mJ, $F = 390$ mm (solid line) and 60 mm (dash line), S-2000 spectrometer (b).

The physical mechanism of Δ_λ behavior is connected with the phase self-modulation of a light wave propagating in the medium with nonlinearity of the Kerr and plasma types. The qualitative consideration of the given phenomenon¹⁴ has shown that spectral broadening of the ultrashort laser pulse in the beam filamentation zone is proportional to the effective length of filament L_F : $\Delta_\lambda(z = L_F) \sim KL_F$, where K is a certain coefficient depending on nonlinear properties of the medium. Since the filament length at a fixed propagation geometry is proportional to the initial radiation power, Δ_λ also increases due to the beam power increase.

The quantity of Δ_λ depending on relative length of beam filamentation L_F/L_R (where $L_R = \pi R_0^2/\lambda_0$ is the Rayleigh length; R_0 is the beam radius at the level e^{-1} of the intensity maximum) is presented in Fig. 3.

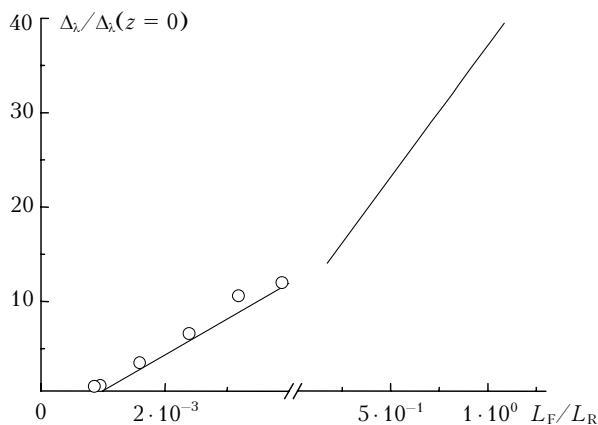


Fig. 3. Theoretical and experimental data on spectral half-width dependences of SC radiation on the relative length of the femtosecond beam filamentation focused by the mirror with $F = 860$ mm. Symbols denote the experiment, solid line denotes the theoretical calculation.

The data are presented in the normalized form in order to show the tendency in the half-width change of the femtosecond pulse spectrum at rather large L_F , where there are no experimental results available at present. The theoretical calculation was conducted within the limits of the radial-symmetrical model of radiation filamentation, when one axial filament is formed. Nevertheless, the theoretical modeling gives a valid interpretation of the experimental data and points out that preferred growth of the spectral pulse width occurs just in the beam filamentation zone, where its intensity is maximum, and the value of Δ_λ is proportional to the zone length.

Effective radius of a light beam

In order to track the evolution of a laser beam dimension subjected to the self-focusing in the air, the recording of energy density profiles $W(x, y)$ was carried out at six points along the optical path. The digitized values of the photodetector array illumination, characterizing the density distribution of radiation energy, were filtered and processed in a computer so that to determine R_e by the formula (1).

Figure 4 presents the cross section of a femtosecond laser beam, passed through the filamentation area. Bright glowing areas represent radiation of the filamented part of the beam, and the darker halo represents the peripheral zones, which are not subjected to the self-focusing.

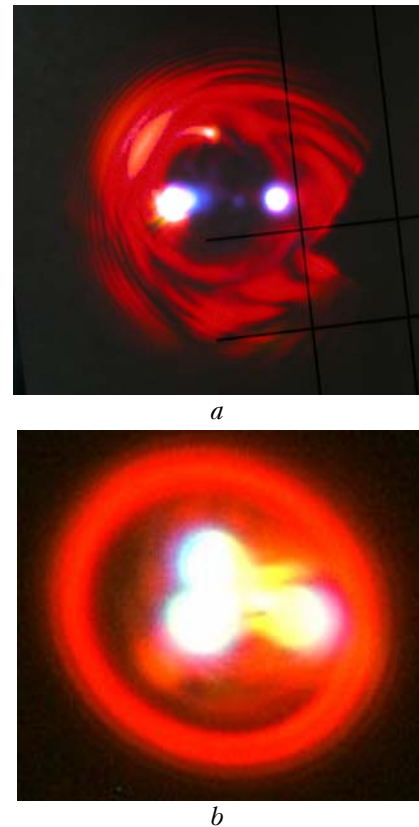


Fig. 4. Image of a filamented laser beam: at mirror focusing $F = 860$ mm, $E_0 = 8$ mJ, $t_p = 80$ fs, survey by the camera Sony-DSC-F828, side of the square 1.25 cm (a); at focusing with $F = 400$ cm, $E_0 = 18$ mJ, $t_p = 50$ fs, survey by the camera Nikon D70 (b).

The values of R_e obtained from the experimental measurements along the beam path, are brought together with theoretical calculations of the given value, carried out for the experimental conditions (Fig. 5). The data are presented for the whole range of radiation energies realized in the experiment ($E_0 = 0.1\text{--}14$ mJ), when one filament had appeared (dark points) and several filaments (light), and the measurements of R_e at source operation in a nanosecond mode without nonlinear interaction along the path.

Reference 14 shows that self-action of a femtosecond beam is expressed in higher angular radiation divergence after the passage of the global nonlinear focus. It takes place due to the change in the beam spatial profile (filamentation), and in the nonlinear modulation of wave phase formed by the plasma channel inducing defocusing of the pulse trailing edge. Nevertheless, in all cases, presented in Fig. 5, the experimental data can be quite accurately reduced to one curve constructed by the expression for the effective radius by means of a special scaling

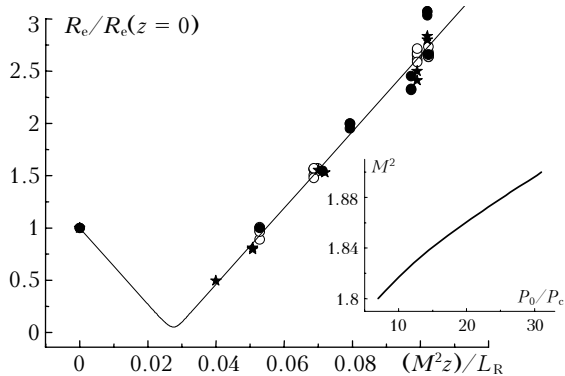


Fig. 5. The effective radius dependence of the filamented femtosecond beam on the reduced propagation distance: \circ is the multiple filamentation; \bullet is the single filamentation; \star is the linear condition; solid line denotes the calculation by formula (2). On the right, the beam propagation factor M^2 is shown as a function of the initial radiation power (calculation using the experimental data).

$$R_e(z) = \sqrt{R_{ew}^2 + \frac{(z - z_w)^2}{(L_R/M^2)^2}}, \quad z > z_w, \quad (2)$$

where $R_{ew} = R_e(z = z_w)$ is the effective beam radius in the focal beam waist with the coordinate z_w ; $M^2 \geq 1$ is the coefficient of beam propagation.

Note that the Gaussian beam ($M^2 = 1$) has minimum value of this factor and the higher the values M^2 , the stronger the difference of the intensity cross profile from the Gaussian shape. The scaling parameters in Eq. (2) are the values of R_{ew} , z_w , and M^2 , which are the functions of the initial radiation power. The values of M^2 are obtained from the experimental data. The initial pulse power P_0 (see Fig. 5) is normalized to the value of the critical power of radiation self-focusing in the air $P_c = 3.2$ GW. Note that for the mode of nanosecond radiation propagation (linear propagation), $M^2 = 1.1$ owing to the systematic error at cross profile reconstruction of the beam energy density from the photographic information.

As follows from Fig. 5, the experiment did not reveal any apparent differences in behavior of effective light beam dimension under conditions of multiple and single filamentation, in spite of the cardinal differences in cross density distribution of radiation energy. This shows that dynamics of the given filamentation scenarios is similar from the point of view of averaged effective beam radius, starting from formation in the medium of a nonlinear lens, entering into the condition of waveguide propagation and ending by free diffraction behind the linear focus. These experimental results point out the possibility of a versatile description of nonsteady self-action of ultrashort laser radiation pulses in the air based on formalism of its effective characteristics.

Conclusion

The filamentation effect of the high-power laser pulse at its focusing in the air and droplet media has

been studied experimentally and theoretically. It is shown that nonlinear condition of ultrashort radiation effect with water aerosol does not affect the value of beam energy attenuation. The similarity of self-action of the femtosecond focused Gaussian beams of different initial power in the air from the standpoint of evolution has been experimentally found for the first time for their effective characteristics: root-mean-square beam radius and width of the radiation frequency spectrum. The similarity manifests itself in generality of scenario development of single and multiple light beam filamentation, starting from formation in the nonlinear lens medium, entering into condition of waveguide propagation and ending by the radiation linear propagation behind the nonlinear focus. It is shown experimentally and theoretically that increase in the size of the light beam filamentation region induces the increase in effective width of radiation frequency spectrum.

Acknowledgements

This study was supported in part by the Russian Foundation for Basic Research, Grants Nos. 06–02–16300 and 06–05–64799, Complex integration project 3.13 of the Presidium SB RAS.

References

1. S.A. Akhmanov, V.A. Vysloukh, and A.S. Chirkin, *Optics of Femtosecond Pulses* (Nauka, Moscow, 1988), 312 pp.
2. S.N. Bagaev, *Usp. Sovr. Radioelektron*, Nos. 5–6, 70–85 (2004).
3. A.A. Babin, A.M. Kiselev, A.M. Sergeev, and A.N. Stepanov, *Quant. Electron.* **31**, No. 7, 623–626 (2001).
4. V.P. Kandidov, O.G. Kosareva, E.I. Mozhaev, and M.P. Tamarov, *Atmos. Oceanic Opt.* **13**, No. 5, 394–401 (2000).
5. N.N. Bochkarev, A.A. Zemlyanov, A.I. Zemlyanov, A.M. Kabanov, D.V. Kartashov, A.V. Kirsanov, G.G. Matvienko, and A.N. Stepanov, *Atmos. Oceanic Opt.* **17**, No. 12, 861–864 (2004).
6. N. Khan, N. Marium, I. Aris, and J. Yeak, *New J. of Phys.* **4**, 61.1–61.20 (2002).
7. P. Rairoux, H. Schilling, S. Niedermeier, M. Rodriguez, F. Ronneberger, R. Sauerbrey, B. Stein, D. Waite, C. Wedekind, H. Wille, and L. Wöste, *Appl. Phys. B* **71**, No. 4, 573–580 (2000).
8. A.A. Zemlyanov and Yu.E. Geints, *Atmos. Oceanic Opt.* **19**, No. 9, 693–699 (2006).
9. C.C. Cheng, E.M. Wright, and J.V. Moloney, *Phys. Rev. Lett.* **87**, No. 21, 213001–4 (2001).
10. Q. Luo, S.A. Hosseini, W. Liu, J.-F. Gravel, O.G. Kosareva, N.A. Panov, N. Aközbe, V.P. Kandidov, G. Roy, and S.L. Chin, *Appl. Phys. B* **80**, No. 1, 35–38 (2005).
11. J. Kasparian, R. Sauerbrey, D. Mondelain, S. Niedermeier, J. Yu, J.-P. Wolf, J.-B. Andre, M. Franco, B. Prade, S. Tzortzakis, A. Mysyrowicz, M. Rodriguez, H. Wille, and L. Wöste, *Opt. Lett.* **25**, No. 18, 1397–1399 (2000).
12. P. Sprangle, J.R. Peñano, and B. Hafizi, *Phys. Rev. E* **66**, No. 4, 046418 (2002).
13. A.A. Zemlyanov and Yu.E. Geints, *Atmos. Oceanic Opt.* **18**, No. 7, 514–519 (2005).
14. A.A. Zemlyanov and Yu.E. Geints, *Atmos. Oceanic Opt.* **20**, No. 1, 32–39 (2007).